Science Bulletin of National Chiao Tung University, Vol. VI, No. 1

RADIAL PARTICLE LOSS IN A HIGHLY IONIZED CYLINDRICAL PLASMA COLUMN

K. C. HUANG

College of Engineering, National Chiao Tung University

and

K. CHUNG and E. LEVI

Polytechnic Institute of Brooklyn, Farmingdale, N. Y. 11735

(Received October 15, 1972)

Abstract—*The statistical properties of the plasma fluctuations in a long plasma column produced by a hollow cathode arc discharge show that there exist different states of weak plasma turbulence. The transition between these states occurs as a result of changes in the confining magnetic field, the background gas pressure, and the boundary conditions. Associated with such transitions are radial changes in the plasma confinement. A sudden jump in the radial particle loss rates is manifested by the increase of the current collected by Buchelnikova ring-collectors and by the change in the radial density profiles measured by electrostatic probes.*

A linear stability analysis identifies the weak turbulence with the unstable electrostatic ion-cyclotron mode. This mode appears to be unstable in the parameter regions where the inverse gradient length, $\hat{\kappa}$, the perpendicular wave number $k_\perp$ and the ion Larmor radius ρ_H at the sum temperature T_e+T_i are related as $1/\rho_H \gtrsim \kappa \gtrsim k_\perp$. The radial particles loss rate predicted by this analysis agrees with the observed one.

1. INTRODUCTION

Although the first experimental study on the anomalous transport of plasma across the confining magnetic fields was carried out in a low pressure arc discharge by Bohm *et al*,[1] the understanding of the physical processes associated with the anomalous transport in arc-type plasmas is on a less firm ground and at a less sophisticated level when compared to the understanding of other types of plasmas, such as positive columns and alkali plasmas. This situation is caused by several reasons: (1) it is more difficult to control arcs than other plasmas (2) arcs are not easily accessible to such simple and reliable diagnostic tools, as the electrostatic probes (3) the ions are not in thermal equilibrium with the electrons (4) end-effects play a major role in arcs (5) Coulomb collisions are usually dominant for the electrons, whereas collisions with the neutrals are mostly significant for the ions.

Renewed interest in arc type plasmas was, however, generated by the discovery of the high vacuum hollow-cathode arc discharge[2]. In plasma columns generated by

hollow-cathode-arcs, one can get highly ionized (up to 95% on the axis), moderate temperature ($T_e \lesssim 10$ eV, $T_i \sim 1$ eV), moderate density ($n_e \sim 10^{13}-10^{14}$ #/cc) plasmas, which are quite reproducible and controllable. Furthermore relatively quiescent plasmas can be obtained at higher densities than those of quiescent alkali plasmas devices.[3] Of particular significance is the possibility of obtaining an arc plasma in both the quiescent and weak turbulent states, since it affords identification of the roles which plasma fluctuations play in determining the gross features of the plasma structure.

Plasma fluctuations above the thermal level are caused by instabilities of one type or another and, in confined plasmas, are closely related to anomalous diffusion or enhanced particle loss. Especially there has been much interest in low frequency instabilities in inhomogeneous plasma columns. Charged particles cross over the confining magnetic field, B_0, as a result of $E \times B_0$ drifts, where E is the fluctuating electric field. In the presence of an in-phase component of density fluctuations, n, this motion produces a steady and unidirectional flux.

In hollow-cathode produced plasmas, various types of low frequency unstable modes are observed: resistive drift[4], ion acoustic[5], and electrostatic ion-cyclotron[6] instabilities. These waves have several common characteristics: (1) they are electrostatic, i.e., $E = -\nabla\varphi$, (2) the characteristic frequencies ω are lower, or in the order of the ion cyclotron frequency, $\omega \leq \omega_{ci}$, (3) the dynamics of these instabilities are adequately described by the two-fluid equations, and (4) $\omega_{ce}\,\tau_e \gg 1$, while $\omega_{ei}\,\tau_i$ may be as low as unity, where τ_e and τ_i represent electron and ion collision times respectively. Which of these instabilities are important in causing the anomalous transport and what fraction of the pump-out rate is associated with these instabilities are the questions relevant to the problem of plasma confinement.

In this paper we wish to report experimental observations and theoretical explanations of the role of the electrostatic ion-cyclotron instability in the enhanced plasma loss rate across the magnetic field. In Sec. 2, the experimental arrangements, including the plasma device and diagnostic methods, are described. In Sec. 3 the experimental observations on the instability and on the radial loss rates are presented. In Sec. 4 a theory based on two-fluid equations is derived to describe the instability and evaluate the transport rate. The theory of Sec. 4 is compared to the experimental observations in Sec. 5 and the relevance of the theory to our experimental setup is briefly discussed.

2. EXPERIMENTAL ARRANGEMENT

a. Device

The hollow-cathode-arc plasma used in this experiment is produced in a 2 m long vacuum chamber, as shown in Fig. 1. The 15 cm diameter stainless steel vacuum chamber is separated into two sections, source region and drift region, by a baffle, to which is attached a tubular anode (2.54 cm i.d. and 7.62 cm long). The baffle enables us to maintain a very low neutral pressure in the drift region through a differential pumping mechanism. The experiments are performed in the drift region, where various plasma diagnostics tools are located.

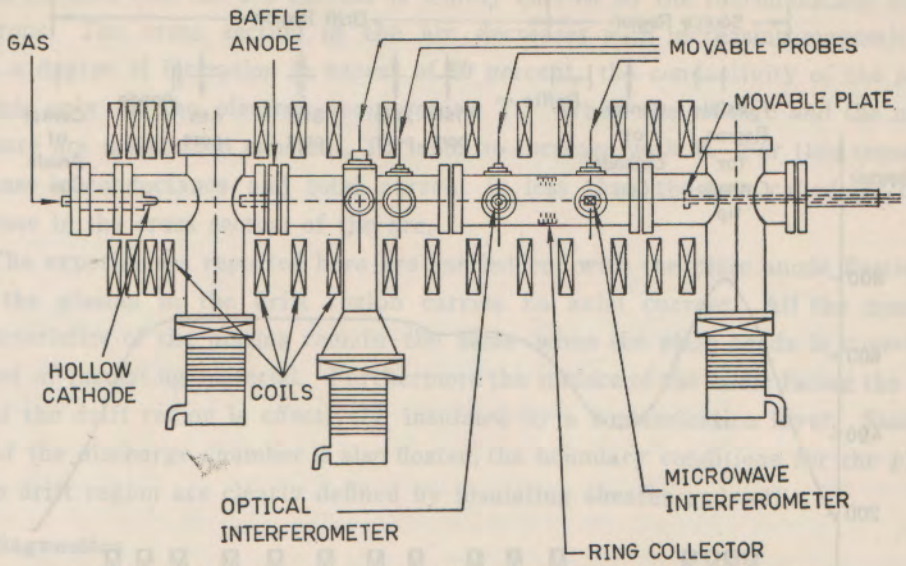

Fig. 1. Arrangement of the hollow-cathode-arc (HCA) system.

The plasma is produced in a 0.125 cm i. d., 10 cm long tantalum cathode through which argon gas is leaked into the chamber. The gas pressure decreases toward the orifice of the hollow cathode and at some interior point the product pd (p=pressure of the gas, d=interior diameter of the cathode tube) is suitable for striking a high current arc. In the cathode the radiation, the ions, and the excited neutrals are trapped together and they heat the cathode to a temperature exceeding 2500°K. The electrons are produced by thermionic emission augmented by field emission and secondary emission. The plasma formed inside the cathode has a density in excess of $5\times10^{14}\,cm^{-3}$ and the ions are 99 percent or more singly ionized. This intense internal plasma is the main source for the lower density external plasma, which extends from the cathode, through the baffle anode, to a movable plate in the drift region. The movable plate can be used as an anode, and the baffle anode can be also floated to function only as a limitor.

A vacuum of up to $\sim10^{-7}$ Torr is maintained in the drift region where the confining magnetic field is uniform within 1 percent and can reach an intensity of 2.6 kGauss. A typical magnetic field configuration along the axis of the plasma column is shown in Fig. 2. The magnetic field in the source region is the typical mirror field previously used in earlier hollow cathode arc devices. Therefore, when the movable plate is floated, the experimental situation in the drift region is similar to that of single ended Q-machines except that the plasma source is a hollow cathode arc.

For a stable arc operation and prompt arc ignition, it is important to locate the cathode tip just after the maximum field point in the source region. When the tip is behind the maximum field point, we observe a violently unstable arc column. If the operating parameters are correct (typical cathode feed rate ≡ 1.0 atm-cc/sec of argon, magnetic field near the cathode tip ≡ 1 kGauss), the arc can be ignited instantaneously on the application of the breakdown oscillator. When a fine copper

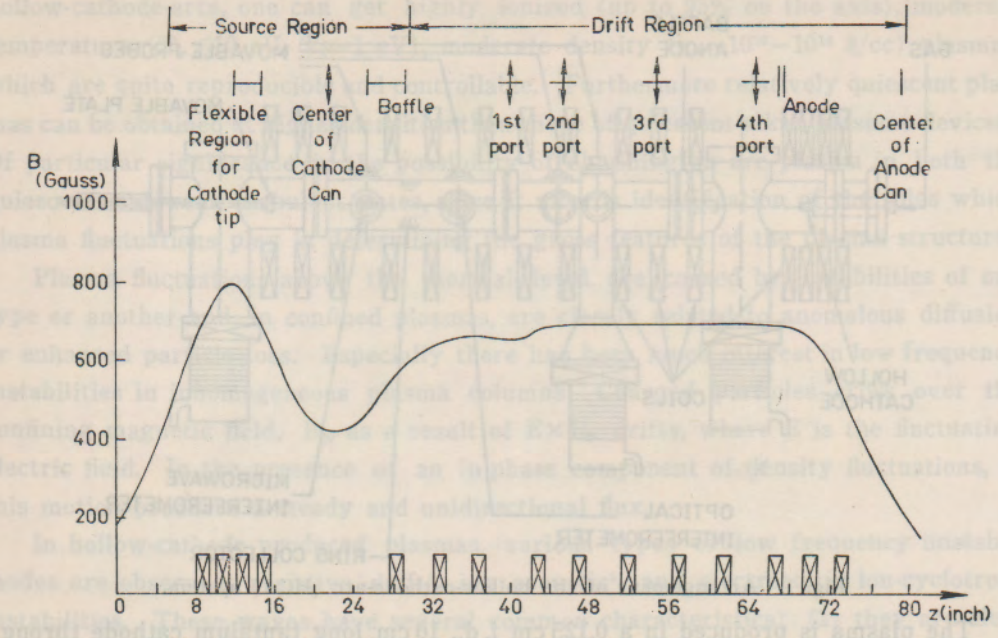

Fig. 2. Axial profile of the magnetic field in the HCA system (Solenoid coil current I_M=100 amp ⇐⇒ B=680 Gauss).

mesh is placed over the baffle-anode, the ignition is easily obtainable, even if the operating conditions are slightly off from the optimum conditions.

The V-I characteristics of the argon arc with grounded plate anode and for typical values of magnetic field and gas feed rate are shown in Fig. 3. The positive

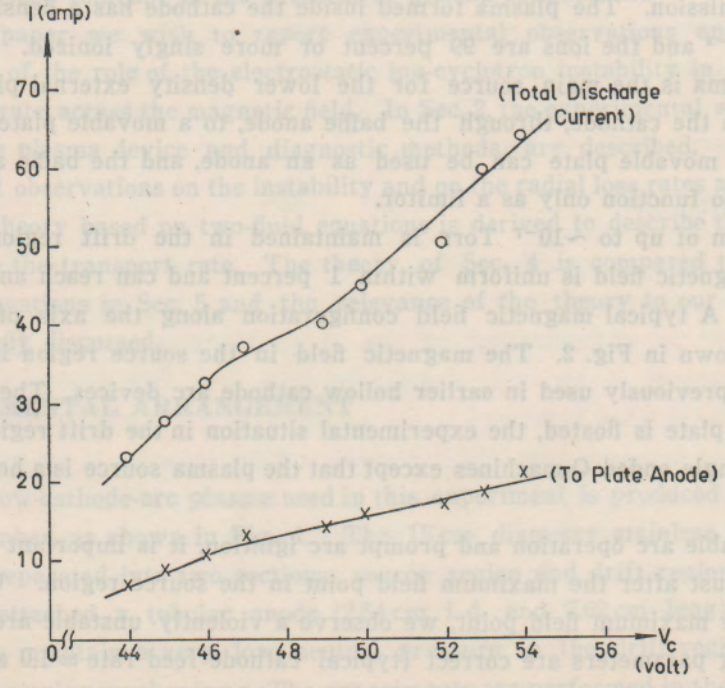

Fig. 3. Discharge currents as a function of the cathode voltage (B=1462.5 Gauss, Q_c=48.3 atm cc/min Q_a=7 atm cc/min).

slopes indicate that the arc current is mainly carried by the thermionically emitted electrons. The cross section of the arc decreases with increasing magnetic field. With a degree of ionization in excess of 90 percent, the conductivity of the plasma depends only on the electron temperature T_e. When the voltage and the neutral pressure are maintained constant, T_e tends to increase with B. For this reason the decrease in conductance and total current is less than the one called for by the decrease in the cross section of the arc.

The experiments reported here are carried out with the plate anode floating, so that the plasma in the drift region carries no axial current. All the measured characteristics of the plasma remain the same when the plate anode is covered by a sheet of insulating material. Furthermore the surface of the baffle facing the other end of the drift region is effectively insulated by a contamination layer. Since the rest of the discharge chamber is also floated, the boundary conditions for the plasma in the drift region are clearly defined by insulating sheaths and walls.

b. Diagnostics

The local plasma density and electron temperature are measured by Langmuir probes 0.254 mm in radius and 6.35 mm in length. A family of Langmuir probe curves were obtained at different radial positions with various magnetic field values. These curves have been analyzed according to Allen, Boyd, Raynold's theory.[7]

Ion temperatures are determined from Doppler broadened line profiles of Ar II line at 4806 Å measured by a Fabry-Perot interferometer. The ion temperature is also determined indirectly from the energy balance equation between electrons, ions and neutrals.

The absolute calibration of the Langnmuir probe measurements is verified by a 60 GHz microwave interferometer, which measures the total number of electrons between two horns. By making use of the radial plasma density profiles obtained from probe measurement, one can determine the peak density of the plasma column.

Information on the plasma fluctuations can be obtained by means of Langmuir probes, light intensity measurements and transmitted microwaves. Most useful is the detection of fluctuations by means of floating and negatively biased Langmuir probes. The fluctuation in the floating potential is representative of the fluctuation in the space potential, since the collisional energy relaxation time is typically 0.1 μ sec, while the characteristic fluctuation time is 10 μ sec. Therefore, the temperature fluctuation, T_e, is small, and the space potential fluctuation, φ_p, is the same as the floating potential fluctuation φ_f. The level of fluctuations in plasma density n can be derived from the current fluctuations i of the negatively biased probes, according to Robinson and Rusbridge.[8] They showed that to a good approximation,

$$\frac{\langle i^2 \rangle}{i_o^2} \approx 0.64 \frac{\langle n^2 \rangle}{n_o^2} \qquad (1)$$

when the bias voltage setting is $\varphi_o = 2.2 \left(\frac{k\,T_e}{e}\right)$ V. The subscript o denotes here the average value.

Probe measurements of the radial profiles of plasma density may also yield information on the radial loss rate of plasma across the magnetic field. Assuming that the longitudinal axial (z) density variation can be neglected and that the loss process is ambipolar, Bohm[1] obtained a relation between the effective perpendicular diffusion coefficient, D_{e-f} and the e-folding distance for the radial density profile, q_L;

$$D_{e-f} = \frac{\alpha}{L}\left(1+\frac{T_i}{T_e}\right)^{-1} q_L^2 \qquad (2)$$

where α is the mean velocity of the electrons which penetrate through the space charge sheath and is equal to the Bohm velocity $(k_B T_e/m_i)^{1/2}$, L is the length of the discharge column. T stands for the temperature and m for the mass of the particle.

We, however, rely primarily on the ring collector technique used by Buchelnikova et al.,[9] in order to measure directly the radial loss of particles in the experimental region. As shown in Fig. 4, the ring collector consists of four rings of which the outer two are floating with respect to the plasma and serve as guard-rings. The inner two rings are connected to a variable voltage source. At low values of biasing potential, the thickness of the sheaths is much smaller than the spacing between the rings, d, the plasma is effectively shielded from the applied field, and the two rings function like a double electrostaic probe. As the potential is increased the positive and negative sheaths overlap and the collected current saturates at a level corresponding to the ambipolar flux of particles entering within the two rings. If R_1 denotes

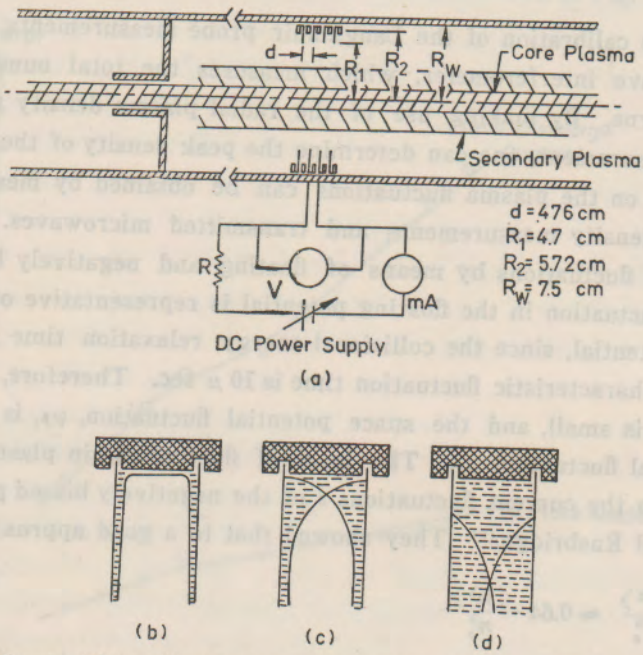

Fig. 4. Ring collector for measurement of the radial flux (a) overall arrangement, (b), (c) and (d) detail of the inner ring showing the effect of growth of the plasma sheath with increasing potential.

the inner radius of the ring, the ambipolar radial flux density Γ_r is related to the saturation current I_s as

$$\Gamma_r\ (R_1) = \frac{I_s}{2\pi\ R_1\ d} \qquad (3)$$

3. OBSERVATIONS

a. Ring-collector measurements

The radial flux measurement by the ring collector exhibits a distinctive feature of the plasma confinement in the hollow-cathode produced plasma column. Typical V-I characteristic curves of the ring collector are shown in Fig. 5. These curves show well defined saturation currents. In Fig. 6, the saturation current is plotted against the magnetic field strength. As expected the general trend is an improvement in confinement with increasing B. However, the curve of Fig. 6 bears also dramatic evidence to the existence of two distinct states separated by a critical value of magnetic field, B_c, in the order of 1 kGauss. At this critical value B_c, a drastic change can also be observed in the appearance of the luminuous part of the plasma, a core which is approximately the geometric extension of the hollow cathode source along the magnetic field lines. The boundary which below B_c is sharp and well defined, becomes diffuse. The transition in the radial flux rate at the critical field strength B_c is closely related to changes in the radial density profiles and plasma fluctuations levels. In fact B_c signifies the transition from a quiescent plasma state to a weakly turbulent plasma state, which, as will be shown, can be attributed to the electrostatic ion-cyclotron instability.

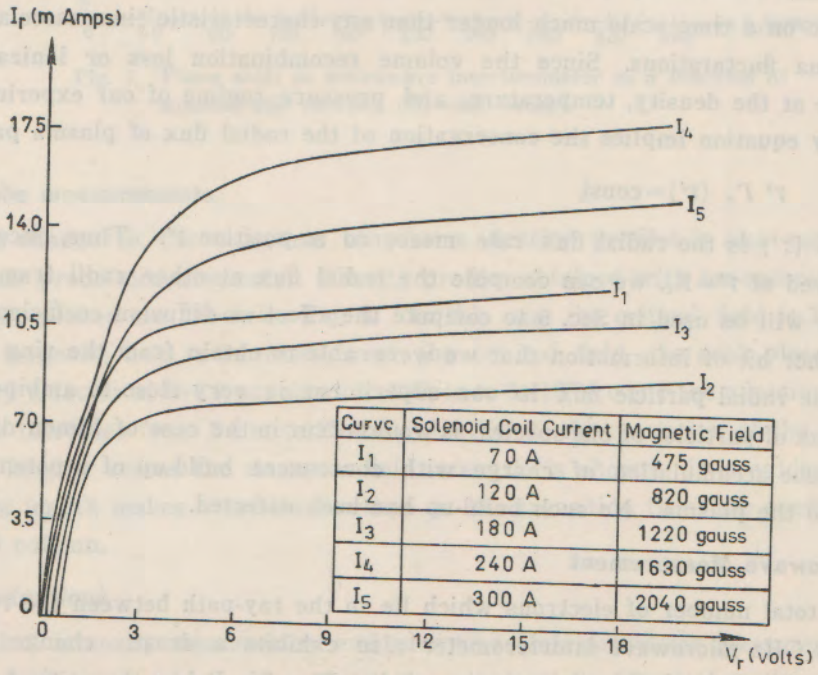

Curve	Solenoid Coil Current	Magnetic Field
I_1	70 A	475 gauss
I_2	120 A	820 gauss
I_3	180 A	1220 gauss
I_4	240 A	1630 gauss
I_5	300 A	2040 gauss

Fig. 5. V-I characteristics of the ring collector at typical values of the confining magnetic field intensity.

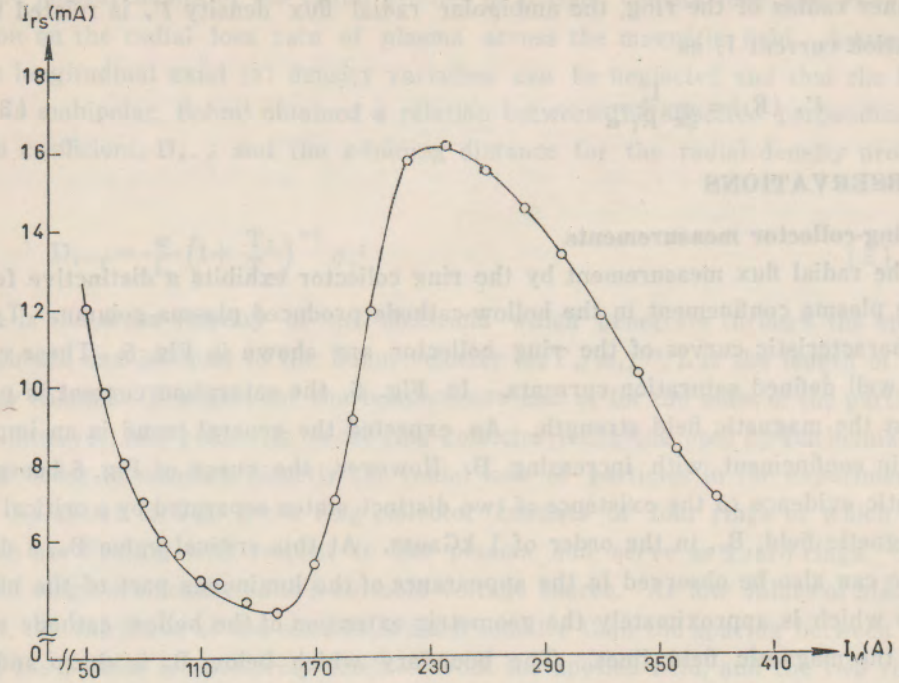

Fig. 6. Ring collector staturation current as a function of solenoid coil current, (B_c=1150 Gauss).

A change in the polarity of the biasing voltage does not cause any change in the characteristic curves of the ring collector, indicating that the plasma column is axially uniform. Also it is safe to assume that the plasma column is azimuthally symmetric on a time scale much longer than any characteristic time associated with the plasma fluctutations. Since the volume recombination loss or ionization are negligible at the density, temperature, and pressure regime of our experiment, the continuity equation implies the conservation of the radial flux of plasma particles,

$$r' \Gamma_r (r') = \text{const} \qquad (4)$$

where $\Gamma_r (r')$ is the radial flux rate measured at position r'. Thus, once $\Gamma_r (R_1)$ is measured at $r' = R_1$, we can compute the radial flux at other radii from Eq. (4). This flux will be used in Sec. 5 to compute the effective diffusion coefficient.

Another bit of information that we were able to obtain from the ring collector is that the radial particle flux in our experiment is very close to ambipolar. An excess flux of particles of one species, as would occur in the case of Simon diffusion[10], would cause accumulation of charge with consequent build-up of a potential with respect to the plasma. No such build-up has been detected.

b. Microwave Measurement

The total number of electrons which lie in the ray-path between the two horns of the 60 GHz microwave interferometer also exhibits a drastic change near the critical magnetic field B_c, as is indicated by Fig. 7. Below the critical magnetic field, the cross sectional number of electrons is more than twice the corresponding

number above the critical magnetic field. It should be noted that the critical magnetic field in Fig. 7 lower than the critical magnetic field in Fig. 6. This difference results from a difference in the background pressure, which is controlled by the cathode gas feed rate and pumping speed. As we shall see in Sec. 5 the threshold for instability and the transitional characteristics at the critical magnetic field depend on the background pressure mainly because the latter controls the electron temperature T_e. The experiments of Fig. 7 were performed with higher pumping speed and, therefore, lower background pressure and higher electron temperature. Under these cenditions the transition from a quiescent to a turbulent state not only occurs at lower B_c, but also much more rapidly.

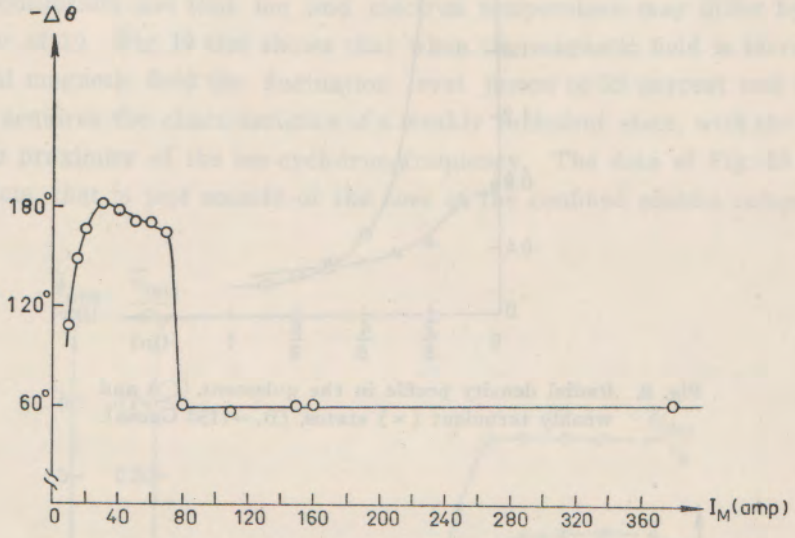

Fig. 7. Phase shift in microwave interferometer as a function of solenoid coil current, (B_c=630 Gauss).

c. Probe measurements

The change in the structure of plasma density profiles is also confirmed by Langmuir probe measurements. Density profiles obtained with ion-saturation-biased Langmuir probes are shown in Fig. 8. In this case the critical field is 1150 Gauss. As the magnetic field is increased over the critical field, the peak plasma density drops by a factor of five from about 4×10^{13}/cc to 8×10^{12}/cc and the minimum *e*-folding distance increases from 3 mm to 25 mm. In Fig. 9, the variation of the average *e*-folding lengths versus the magnetic field strength is shown. It is evident that the *e*-folding length makes a sudden increase at the transition from the confined to the diffused column.

d. Fluctuations

Optical intensity measurement and microwave interferometer measurement show plasma fluctuations whose characteristics are essentially identical to those observed by Langmuir probes. Many Langmuir probes are simultaneously used to record

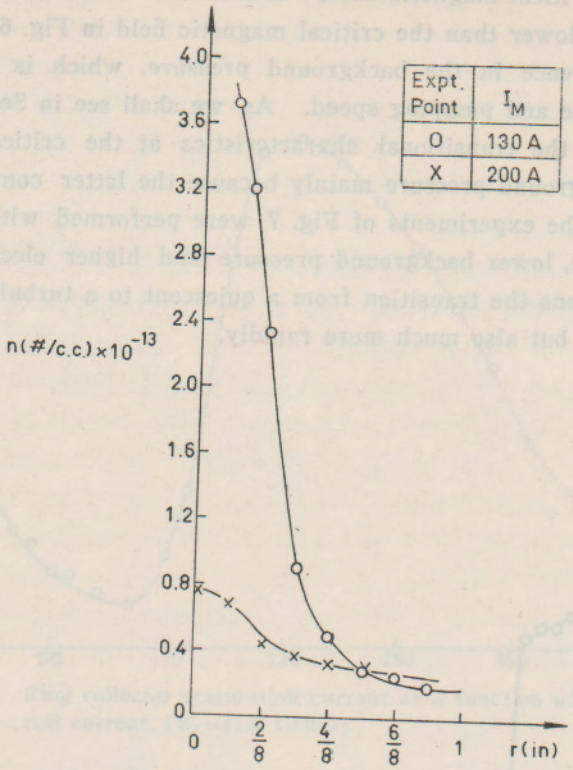

Fig. 8. Radial density profile in the quiescent (○) and weakly turbulent (×) states, (B_c=1150 Gauss).

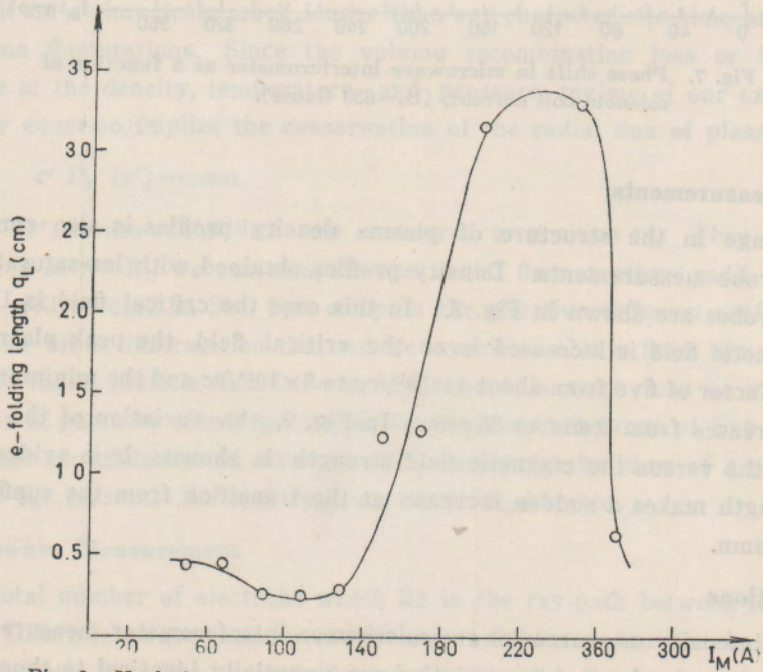

Fig. 9 Variation of the average e-folding length as a function of the solenoid coil current.

potential and density fluctuations. Flutuation signals are recorded on an 8 channel magnetic tape using an Ampex 1300 recorder. Recorded signals are analyzed subsequently by a SAICOR correlation analyzer and a Hewlett Packard spectrum analyzer. Out of these data analysis, we obtain the level of fluctuations, the frequency component of fluctuation spectra, the correlation characteristics of the plasma fluctuations and the propagation characteristics of instabilities.

In Fig. 10, the level of fluctuations is plotted versus the applied magnetic field. The average peak-to-peak potenial fluctuations are presented along with the ratio of mean square root density fluctuation to the average plasma density. Fig. 10 shows that for $B<B_c$ the level of density fluctuations is quite low, approximately 1 percent. In this regime the plasma is practically quiescent, despite the fact that it is far from thermal equilibrium and that ion and electron temperature may differ by as much as a factor of 10. Fig. 10 also shows that when the magnetic field is increased over the critical magnetic field the fluctuation level jumps to 22 percent and the power spectrum acquires the characteristics of a weakly turbulent state, with the dominant line in the proximity of the ion-cyclotron frequency. The data of Fig. 10 are taken at $r=1.25$ cm, that is just outside of the core of the confined plasma column.

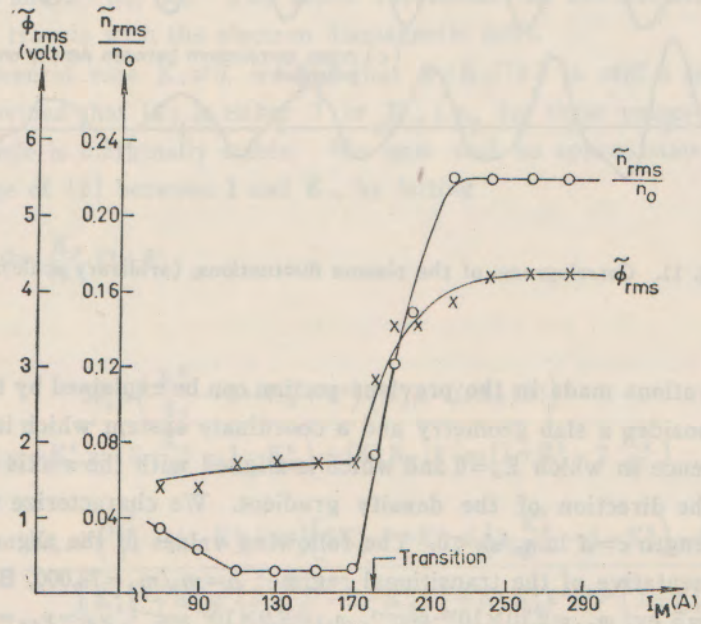

Fig. 10. Density and potential fluctuation levels as a function ot the solenoid coid current ($B_c=1150$ Gauss).

Auto- and cross-correlograms taken in the weakly turbulent plasmas are shown in Fig. 11. Fig. 11(a) is the auto-correlogram of potential fluctuations. The magnitude at $\tau=0$ is the averaged square of the fluctuations. Fig. 11(b) gives the cross-correlogram of the potential fluctuations taken by two floating probes separated by 90° azimuthally. It is evident that these two signals are out-of-phase by 90° indicating that the instability is an $m=1$ mode. The cross-correlogram of Fig. 11(c) between

the potential and the density fluctuations clearly shows that these fluctuations are out of phase with one another. The phase angle between the density and potential fluctuations vary as the magnetic field and the background pressure are varied.

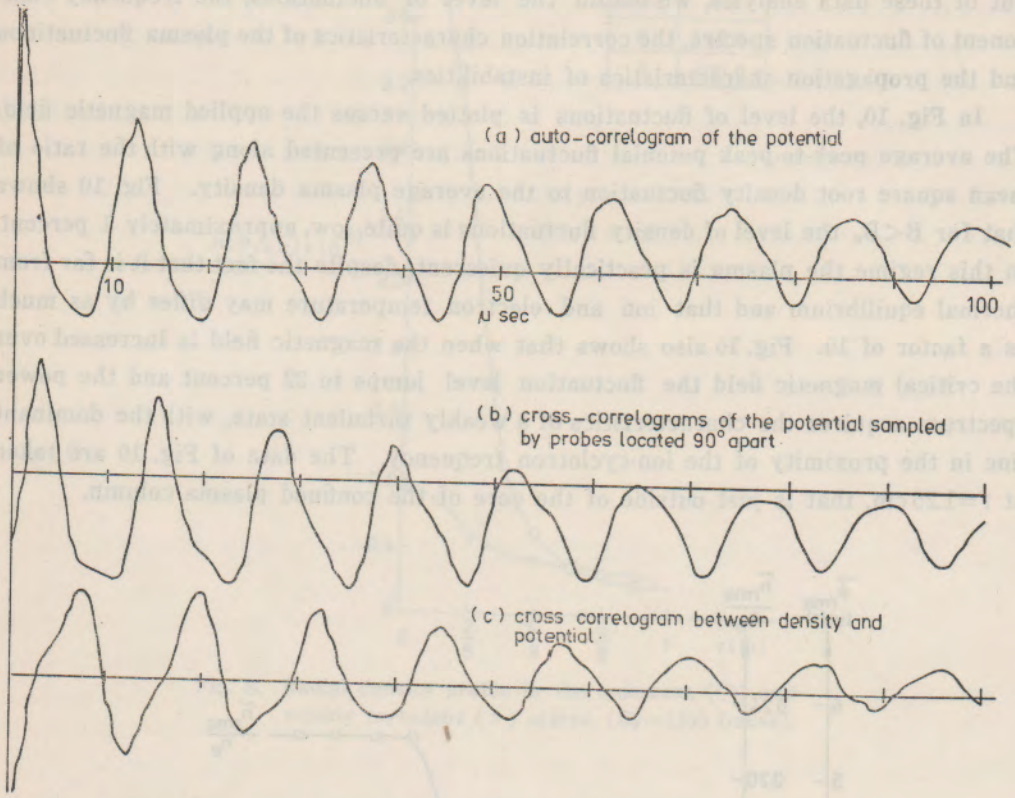

Fig. 11. Correlograms of the plasma fluctuations, (arbitrary scale).

4. THEORY

The observations made in the previous section can be explained by the following theory. We consider a slab geometry and a coordinate system which is fixed to the frame of reference in which $E_o=0$ and which is aligned with the z-axis along B, and the x-axis in the direction of the density gradient. We characterize this gradient by an inverse length $\kappa=d \ln n_0/dx<0$. The following values of the argon plasma are taken as representative of the transitional regime: $\mu=m_i/m_e=73.000$, B=1.2 kGauss, $T_i=0.5$ ev, $T_e=5$ ev, $\omega_{ce}=2.10\times10^{10}$ sec^{-1}, $\omega_{ci}=2.9\times10^{5}$ sec^{-1}, $\nu_{ei}=\nu_{ee}=2\times10^{7}$ sec^{-1}, $\nu_{ii}=3.2\times10^{6}$ sec^{-1}, $\nu_{ie}=2.7\times10^{2}$, sec^{-1}, $\nu_{in}=2\times10^{3}$ sec^{-1}, $a=[k_B(T_e+T_i)/m_i]^{1/2}=3\times10^{3}$ m/sec, $\rho_H=a/\omega_{ci}=10^{-2}$ m, $k_z=3$ m^{-1}, $k_y=n=10^{2}$ m^{-1}, where ν stands for collision frequency, k, for the wave number, the subscript n for neutral and k_B is the Boltzmann coefficient.

Under these conditions the describing parameters satisfy the following inequalities: $\omega\ll\omega_{ce}$, $\omega\ll\nu_{ei}$, $\omega\ll\nu_{ii}$, $v_{th,e}\ll\nu_{ei}/k_z$; $v_{th,i}\ll\omega/k_z$; $\omega_{ce}\gg k_y^2 v_{th,e}^2/\nu_{ee}$; $\omega_{ci}\gg k_y^2 v_{th,i}^2/\nu_{ii}$, $\omega_{ei}\tau_{in}\gg1$, where v_{th} is the thermal speed. Therefore, the analysis can be based on a fluid dynamic representation with the following simplifying assumptions:

(a) neutral plasma, (b) electrostatic and isothermal waves, (c) negligible viscosity and Larmour radius effects for both the electrons and the ions. (d) negligible collisions for the ions, (e) negligible inertia for the electrons.

By making the local approximation in x and by assuming that the perturbations vary as exp $[j(\omega t-k_y y-k_z z)]$, one arrives at the following dispersion relation

$$\Omega^3-A\ \Omega^2-B\ \Omega+C=0 \tag{5}$$

where

$$A=K_y^2\nu\frac{\nu K_y|\hat{\kappa}|+jK_z^2\mu}{\nu^2K_y^2\hat{\kappa}^2+K_z^4\mu^2}$$

$$B=(1+K_y^2)\frac{K_z^4\mu^2-jK_yK_z^2|\hat{\kappa}|\mu\nu}{\nu^2K_y^2\hat{\kappa}^2+K_y^4\mu^2}$$

$$C=K_yK_z^2|\hat{n}|\mu\frac{K_z^2\mu-jK_y|\hat{\kappa}|\nu}{\nu^2K_y^2\hat{\kappa}^2+K_z^2\mu^2}$$

and

$$\Omega=(\omega-k_yv_{ioy})/\omega_{ci},\nu=\nu_{ei}/|\omega_{ci}|$$

$$K=ka/|\omega_{ci}|,\ \hat{\kappa}=na/|\omega_{ci}|$$

We observe that in the limit $K_z=0$, both B and C vanish and we have a double root at $\Omega=0$ and $\Omega=K_y/|\hat{\kappa}|$. The latter represents the electrostatic ion cyclotron mode which travels with the electron diamagnetic drift.

In the general case $K_z\neq0$, we find that $\Omega=K_y/|\hat{\kappa}|$ is still a root of the cubic equation provided that $|\hat{\kappa}|$ is either 1 or K_y, i.e., for these values of $|\hat{\kappa}|$, the ion cyclotron mode is marginally stable. We now seek an approximate solution, valid for the range of $|\hat{\kappa}|$ between 1 and K_y, by letting

$$\Omega=\frac{K_y}{|\hat{\kappa}|}(1+\delta) \tag{6}$$

and find

$$\delta=-\frac{K_z^2\mu\left(\frac{K_y^2}{\hat{\kappa}_2}-1-K_y^2+\hat{\kappa}^2\right)\left(K_z^2\mu-j\nu K_y|\hat{\kappa}|\right)}{K_y^4\nu^3+K_z^4\mu^2\left(3\frac{K_y^2}{\hat{\kappa}^2}-1-K_y^2\right)+jK_z^2K_y|\hat{\kappa}|\mu\nu[1+K_y^2-2\frac{K_y^2}{\hat{\kappa}^2}]} \tag{7}$$

$$\mathrm{Re}(\delta)=-\frac{K_z^4\mu^2\left(\frac{K_y^2}{\hat{\kappa}^2}-1-K_y^2+\hat{\kappa}^2\right)\left[3K_y^4\nu^2+K_z^4\mu^2\left(3\frac{K_y^2}{\hat{\kappa}^2}-1-K_y^2\right)-K_y\hat{\kappa}^2\nu(1+K_y^2)\right]}{\left[K_y^4\nu^2+K_z^4\mu^2\left(3\frac{K_y^2}{\hat{\kappa}^2}-1-K_y^2\right)\right]+K_z^4K_y^2\hat{\kappa}^2\mu^2\nu^2\left[1+K_y^2-2\frac{K_y^2}{\hat{\kappa}^2}\right]^2}$$

$$\mathrm{Im}(\delta)=\frac{K_z^2K_y^3|\hat{\kappa}|\mu\nu\left(\frac{K_y^2}{\hat{\kappa}^2}-1-K_y^2+\hat{\kappa}^2\right)\left(\frac{K_z^4\mu^2}{\hat{\kappa}^2}+\nu K_y\right)}{\left[K_y^4\nu^2+K_z^4\mu^2\left(3\frac{K_y^2}{\kappa^2}-1-K_y^2\right)\right]^2+K_z^4K_y^2\hat{\kappa}^2\mu^2\nu^2\left[1+K_y^2-2\frac{K_y^2}{\hat{\kappa}^2}\right]^2} \tag{8}$$

We observe that for $|\hat{\kappa}|$ between 1 and K_y, $\left(\frac{K_y^2}{\hat{\kappa}^2}-1-K_y^2+\hat{\kappa}^2\right)$ and therefore $\mathrm{Im}(\delta)$ is always negative, thus denoting instability. Outside this interval the cyclotron wave is damped.

When the cyclotron wave is marginally stable $\left(\Omega=\frac{K_y}{|\hat{k}|}\right)$ the other two roots of the cubic are given by

$$\Omega^2+\left(\frac{K_y}{|\hat{k}|}-A\right)\Omega+\frac{K_y^2}{\hat{k}^2}-\frac{K_y}{|\hat{k}|}A-B=0 \tag{9}$$

so that

$$\Omega=\frac{A-K_y/|\hat{k}|}{2}\pm\sqrt{\left[\frac{A-K_y/|\hat{k}|}{2}\right]^2+B+\underbrace{\frac{K_y}{|\hat{k}|}A-\frac{K_y^2}{\hat{k}^2}}_{C|\hat{k}|/K_y}}$$

$$=\frac{\left[K_yK_z^2\mu\left(-\frac{K_z^2\mu}{|\hat{k}|}+j\nu\right)\pm\sqrt{K_y^2K_z^4\mu^2\left(-\frac{K_z^2\mu}{|\hat{k}|}+j\nu\right)^2+4K_z^2\hat{k}^2\mu\left(\nu^2K_y^2\hat{k}^2+K_z^4\mu^2\right)\left(K_z^2\mu-jK_y|\hat{k}|\nu\right)}\right]}{2(\nu^2K_y^2\hat{k}^2+K_z^4\mu^2)} \tag{10}$$

Of these roots one is a cyclotron wave moving in the direction of the ion diamagnetic drift and is damped. The other is a drift wave moving in the direction of the electron dimagnetic drift and is unstable.

According to Chen,[11] the fluctuations in density reach saturation when $\partial n/\partial y=\partial n_o/\partial x$, where $\partial n_o/\partial x$ is the prevailing density gradient averaged over the eddies in the tubulent state. For the $m=1$ mode we have $|\kappa|\approx k_y$, so that $n_{max}\approx n_o$. The observed *rms* value is $n_{rms}=0.22\ n_o$. This indicates that the fluctuations approach the satuation level. On the other hand there is no evidence that nonlinear effects play a dominant role in shaping the fluctuation spectrum or determining the correlation time. The observed spectrum is typical of a weakly turbulent state and the correlation time $\tau_c=10^{-3}$ sec corresponds to the life-time of the ions, as determined by their transit time along the experimental section of the device. For these reasons the diffusion flux might not depart appreciably from that predicted by a linear theory.

The average flux density in the x direction is given by

$$\Gamma_x=\mathrm{Re}\langle v_x\ n\rangle=\mathrm{Re}\left\langle j\frac{k_y\varphi}{B}n\right\rangle \tag{11}$$

From the continuity and momentum equations for the electrons, and assuming an adiabatic drift, we can obtain

$$\varphi=\frac{n}{n_o}\ \frac{j\nu_{ei}\omega_{ce}[\omega m_e-jk_z^2k_BT_{e\|}/\nu_{ei}]}{e(k_z^2\omega_{ce}-j\kappa k_y\nu_{ei}} \tag{12}$$

and

$$\Gamma_x=\mathrm{Re}\left\langle\frac{k_yn^2}{n_o}\ \frac{\left[jk_z^2\frac{k_BT_{e\|}}{m_e}-\omega\nu_{ei}\right]}{k_z^2\omega_{ce}-j\kappa k_y\nu_{ei}}\right\rangle$$

$$= \frac{k_y n^2}{n_o} \frac{\left(\mathrm{Im}(\omega)\nu_{ei} - k_z^2 \frac{k_B T_{e\parallel}}{m_e}\right)\left(\kappa k_y \nu_e\right) - k_z^2 \omega_{ce} \nu_{ei} \mathrm{Re}(\omega)}{k_z^4 \omega_{ce}^2 + \kappa^2 k_y^2 \nu_{ei}^2}$$

$$= \frac{n^2}{n_o} \frac{k_y \nu_{ei}}{k_z^4 \omega_{ce}^2 + \kappa^2 k_y^2 \nu_{ei}^2} \left[\left\{k_z^4 \left(|\kappa| k_y \frac{k_B T_{e\parallel}}{m_e} - \omega_{ce} \mathrm{Re}(\omega)\right)\right\} - |\kappa| k_y \nu_{ei} \mathrm{Im}(\omega)\right] \tag{13}$$

We note that for the unstable mode $\mathrm{Im}(\omega)<0$, however $\mathrm{Re}(\omega)>0$. It follows that the middle term represents pump-in. If we introduce for the ion cycloton

$$\mathrm{Re}(\omega) = K_y\left(\left|\frac{\omega_{ci}}{\hat{\kappa}}\right| - \left|\frac{\kappa}{\omega_{ci}}\right| \frac{k_B T_i}{m_i}\right) \text{ and let } \mathrm{Im}(\omega) \to 0$$

the expression within the $\{\ \}$ brackets reduces to

$$k_z^2 k_y |\hat{\kappa}| \left[\frac{k_B(T_{e\parallel} + T_i}{m_e} - \frac{|\omega_{ci}|\omega_{ce}}{\hat{\kappa}^2}\right] \text{ and for the experimental values of}$$

the parameters the two terms balance out. We thus obtain

$$\Gamma_x \doteqdot \Gamma_r \doteqdot \frac{n^2}{n_o} \frac{k_y^2 \nu_{ei}^2 |\mathrm{Im}(\omega)\hat{n}|}{k_2^4 \omega_{ce}^2 + \hat{\kappa}^2 k_y^2 \nu_{ei}^2} \tag{14}$$

5. DISCUSSION

On the assumption that Fick's law is applicable, the plasma loss across the magnetic field can be characterized in terms of an effective diffusion coefficient $D_\perp = \Gamma_r / |\nabla n|$. We wish to compare $D_\perp$ deduced from the experimental data with those $D_{\perp s}$ predited by various theories.

If the diffusion process is classical and binary collisions are held responsible for the radial particle loss, the following ambipolar diffusion coefficient can be obtained for a three component plasma

$$D_{cl} \cong \frac{k_B(T_e + T_i)}{\frac{e^2 B^2}{m_e \nu_{ei}} + m_i \nu_{in}} \tag{15}$$

This expression is valid when the temperature gradient is negligible, electron-ion coulomb collisions dominate over electron-neutral collisions for electrons, and ion-neutral collisions are important for ions.

When, instead, the diffusion process results from collective interactions, one can check the experimental data against the empirical coefficient of anomalous diffusion derived by Bohm[1]

$$D_B = \frac{k_B T_e}{16 e B} \tag{16}$$

Refinements to this formula have been derived on the basis of the theory of weak turbulence. From Eq. (14) we get an effective diffusion coefficient

$$D_{a.d.} = \frac{n^2}{n_o^2} \frac{k_y^2 \nu_{ei}^2 (\mathrm{Im}(\omega))}{k_z^4 \omega_{ce}^2 + n^2 k_y^2 \nu_{ei}^2} \tag{17}$$

Experimental diffusion coefficients can be deduced from the flux measurements by the ring collector and the measurements of the density gradient by using the formula

$$D_r(r') = \frac{\Gamma_r(r')}{\left(\frac{dn}{dr}\right)_{r'}} \tag{18}$$

where $\left(\frac{dn}{dr}\right)_{r'}$ is the radial density gradient at the radial position r'. In Fig. 12, D_r at $r'=1.25$ cm is plotted against the confining magnetic field. Also plotted and denoted by D_{e-f} is the diffusion coefficient estimated from the e-folding distance measurement, using Eq. (2). It should be noted that the concept of a diffusion coefficient based on Fick's law is applicable only to situations where q_L is large as compared to the ion Larmor radius and small as compared to the e-folding length of the temperature profiles. These conditions are satisfied in the secondary plasmas to which the present considerations refer.

Observing Fig. 12, we immediately see that the effective diffusion is very close to the classical diffusion loss rate, below the critical magnetic field, and reaches Bohm's anomalous diffusion rate, above the critical magnetic field. It is noted that D_r and D_{e-f} are following qualitatively similar patterns. Theoretical predictions of the anomalous diffusion coefficient can also be obtained by introducing appropriate values of the plasma parameters in Eq. (17). The values thus computed by $D_{a.d.}$ in Fig. 12. As we see, they are in satisfactory agreement with the experimental points.

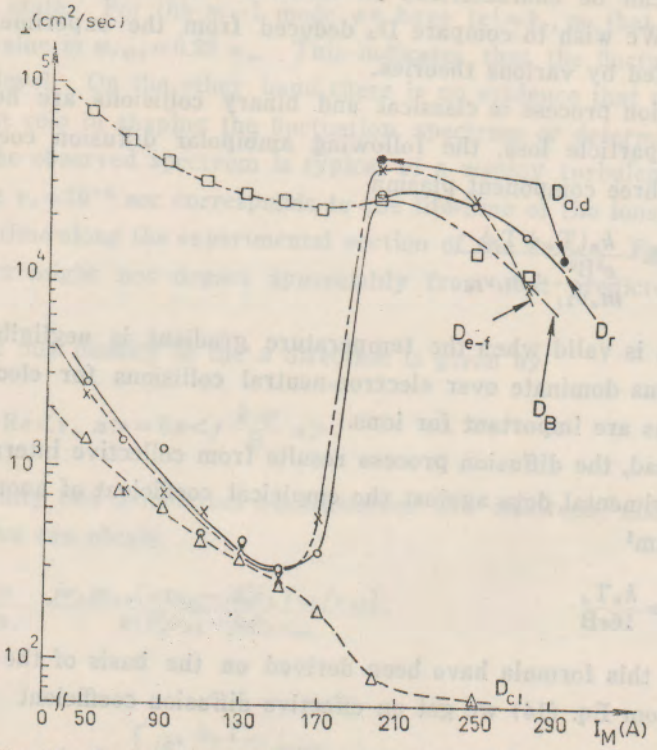

Fig. 12. Perpendicular diffusion coefficients as a function of solenoid coid current ($\gamma=\frac{1}{2}''$, $B_c=1150$ Gauss).

The mechanism which is responsible for the weak turbulence and which causes the transition from the quiescent state was previously identified by Chung and Rose[6] with the electrostatic ion-cyclotron instability. This mode is nearly an $m=1$ mode and propagates across the magnetic field ($k_z/k_y \ll 1$). The dispersion relation obtained in Sec. 4 indicates that this mode can be unstable in the parameter regions wehre the inverse gradient length, κ, the perpendicular wave number $k_\perp$, and the ion Larmour radius ρ_H at the sum temperature T_e+T_i are related as $1/\rho_H \gtrsim \kappa \gtrsim k_\perp$.

Under the conditions of the experiment the lower inequality is satisfied and instability occurs when, with increasing magnetic field, $\kappa\rho_H$ reaches the value of unity. It has been mentioned in Sec. 3b, that the critical magnetic field B_c decreases with the background pressure. The form of Eq. (2) suggests an explanation for this trend. Making use of Eq. (15) and noting that the ν_{in} term is negligible, $\alpha \propto T_e^{1/2}$, and $\nu_{ei} \propto T_e^{-3/2}$, we arrive at the conclusion that $1/q_L = \kappa \propto T_e/\rho_H$, so that $\kappa\rho_H$ is proportional to the electron temperature. As pointed out by Hudis, Chung and Rose[12], in a hollow-cathode arc discharge, T_e increases with increasing B and decreasing background pressure. As a consequence, at lower pressure a lower value of B_c is required for T_e to reach the value which gives rise to the instability.

It must be mentioned at this point that other considerations prevail when the end plate anode is grounded and the plasma in the experimental region carries a strong current. In this case the plasma is stable at a much higher electron temperature. Three stabilizing factors can account for this situation: (1) the tying of the magnetic field lines by the conducting electron-rich sheath which replaces the insulation ion-reach sheath in front of the end plate anode (2) the shear which the presence of an axial current introduces in the confining magnetic field[13], and (3) the ion Landau damping resutling from the higher ion temperature.

Both in the confined and the diffused column, other instabilities e. g. drift and ion acoustic waves may exist and were observed. When the density gradient becomes substantial, we observed a well defined frift wave at the edge of the plasma column. It should be noted, however, that the radial flux measurements indicate that the particle loss rate accompanying the onset of this instabitity is not as significant as in the case of the electrostatic ion-cyclotron instabitity reported above.

ACKNOWLEDGMENT

The experiment was performed at the Polytechnic Institute of Brooklyn. The work was also supported in part by the U. S. Atomic Energy Commission under Contract No. AT(30-1)-3956.

REFERENCES

1. A. Guthrie and R. K. Wakerling, "The Characteristics of Electrical Discharge in Magnetic Fields," McGraw-Hill Co., Inc., New York, p. 200, (1949).
2. L. M. Lidsky, S. D. Rothledger, D. J. Rose and S. Yoshikawa, J. of App. Phys., **33**, 2490, (1962).
3. J. C. Woo and D. J. Rose, Phys. Fluids, **10**, 893, (1967).
4. K. Chung and D. J. Rose, App. Phys. Lett. **11**, 247 (1967).
5. R. L. Gunshor, J. H. Noon and E. H. Holt, Phys. Fluids, **11**, 1763, (1968).

6. K. Chung and D. J. Rose, Proc. of PIBMRI International Symposium on "Turbulence of Fluids and Plasmas," p. 311, (1968).
7. F. F. Chen, Plasma Physics, **7**, 47, (1965).
8. D. C. Robinson and M. G. Rusbridge, Plasma Physics, **11**, 73, (1969).
9. N. S. Buchelnikova, A. M. Kudryotsev and R. A. Salimov, Soviet Physics-Technical Physics, **10**, 53, (1965).
10. A. Simon, Phys. Rev., **98**, 317, (1955).
11. F. F. Chen, Phys. Fluids, **8**, 912, (1965).
12. M. Hudis, K. Chung, and D. J. Rose, J. App. phys., **39**, 3297, (1968).
13. J. N. Davidson, and T. Kammash, Phys. Fludds, **13**, 721, (1970).